LLNL-TR-666420

Detonation Energy Densities from the Cylinder Test

P. C. Souers, P. A. Vitello

January 22, 2015

This work performed under the auspices of the U.S. Department of Energy by Lawrence Livermore National Laboratory under Contract DE-AC52-07NA27344.

Detonation Energy Densities from the Cylinder Test, by P. Clark Souers and Peter Vitello

1. How the Cylinder Test Works

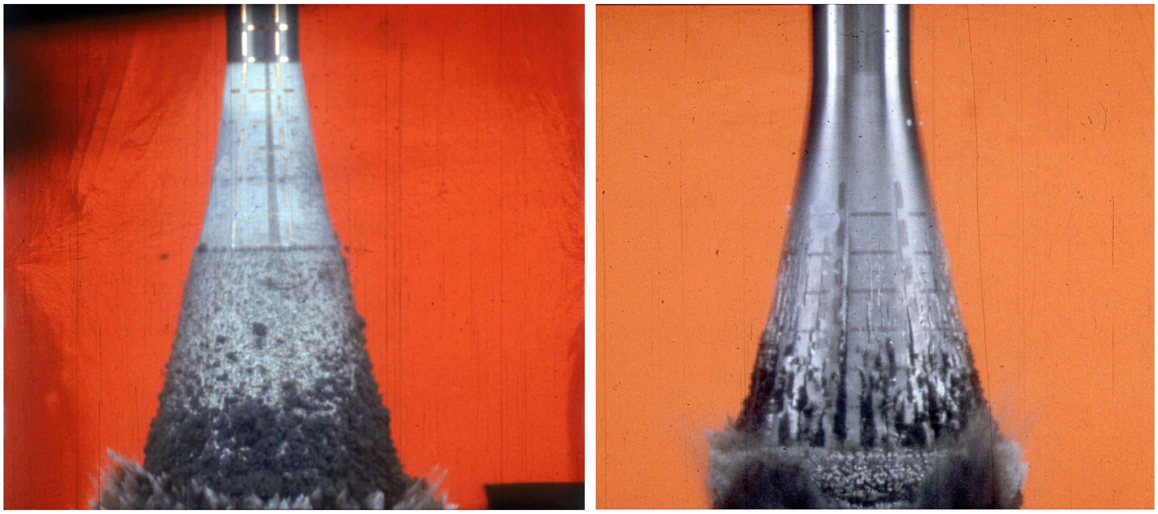

Figure 1a. Two views of an expanding cylinder taken in the Dawn Age of 1964. These are half or less of the normal length. The detonations run upward.

The Cylinder test is a calibrated pipe-bomb used as the only means of obtaining detonation energy densities while the detonation is proceeding [1-2]. The test is close to being a precision test and is no longer the qualitative process found in much of the literature. Most copper tubes have a wall thickness that is $1/5^{th}$ the radius as the standard. The output is an annealed copper wall velocity as a function of time. The square of the velocity is proportional to the detonation energy density, E_d, at a specific relative volume, v. We want to 1) convert copper wall velocity to detonation energy density, 2) have the process be analytical so it can be applied to hundreds of runs at once, 3) have the resulting JWL equation-of-state give a good result when run in a hydrocode, and 4) provide an accurate record for future use.

The whole approach should be as independent of hydrocodes as possible. It should certainly avoid having to run a code for each cylinder shot.

What does scaling mean? It references all size cylinders to a 1-inch diameter. It does this by dividing all times and distances (but not velocities) by the diameter in inches. So, the initial scaled inner cylinder radius is always 12.7 mm. A 4-inch cylinder would be scaled by dividing by 4. The advantage is that all cylinders, hundreds of them at once, can be compared in the same table. The reference is to the inner copper wall, not the explosive, which means there can be an air gap between them.

2. Experimental Details

Table 2a lists the cylinder sizes that have been used at LLNL**.** The copper is oxygen-free OFHC. It should be vacuum-annealed above at least 600°C for two hours with a nitrogen quench. No copper tube should ever be used without having in hand the certificate that states the copper was annealed. A Cylinder test set-up is shown in Figure 2a and its diagram is shown in Figure 2b. The frame has become more robust through the years, especially the aluminum blocks that hold the PDV probes, so we can lock the angle to within one degree. The Lucite bar at the top, despite appearances, lies above and to the right of the top of the cylinder. The cylinder is held only at about a quarter of the way up, with the detonation proceeding upwards. The cylinder should NEVER be held or clamped at the top end.

The copper is oxygen free 101 OFHC, ASTM F68-05. The tubes were purchased from

J3 Associates, Inc
2751 Aiello Drive
San Jose, CA 95111
(508) 281-4412.

They obtained the copper rod from

Sequoia Brass & Copper
2353 Industrial Parkway W.
Hayward, CA 94545.

which in turn came from

Mango Brass & Copper
10930 Sherbrooke Street East
Montreal East, Quebec J1B 1B4

J3 also had the annealing in an inert atmosphere done by

Byington Steel Treating
1225 Memorex Drive
Santa Clara, CA 95050.

We have always used a vacuum anneal, ramped to 590-760° C with a 2-hour soak and a nitrogen quench. A question exists in the literature about one-hour anneals at 600-650°C, where we find final grain sizes of 40 to 240 μm, which means that this temperature may not guarantee a fully annealed sample. It looks as though an hour at 700°C is a better idea, and we are rewriting our specifications for the higher number. Some copper annealing data is shown in Figure 2c [3].

Table 2a. Dimensions and tolerances of all LLNL Copper Cylinders. Full-wall have wall ~ inner radius/5; half-wall have wall ~ inner radius/10.

tab no.	Inner diameter (inches)	ID ± Tolerance (inches)	Wall Thickness (inches)	Wall ± Tolerance (inches)	Length (inches)	Length ± Tolerance (inches)	Type
As listed on the Engineering Drawing, in inches							
15	1.000	0.002	0.1022	0.0005	18.00	0.03	full
14	3.00	0.002	0.300	0.001	30.00	0.03	full
13	0.250	0.002	0.0250	0.0005	6.00	0.03	full
12	2.000	0.002	0.2046	0.0005	18.00	0.03	full
11	0.750	0.002	0.0766	0.0005	9.00	0.03	full
10	1.000	0.002	0.1022	0.0005	12.00	0.03	full
9	0.377	0.002	0.035	0.002	6.00	0.03	full
8	2.0010	0.0005	0.2046	0.0010	12.00	0.03	full
7	0.500	0.002	0.0535	0.0020	6.00	0.03	full
6	8.000	0.005	0.819	0.005	48.00	0.03	full
5	4.001	0.003	0.4094	0.0030	40.00	0.03	full
4	2.0010	0.0002	0.2046	0.0005	12.00	0.03	full
3	2.0010	0.0002	0.1070	0.0002	12.00	0.03	half
2	1.0010	0.0002	0.1022	0.0002	12.00	0.03	full
1	1.0010	0.0002	0.0535	0.0002	12.00	0.03	half
Converted into millimeters, largest down to smallest							
6	203.2	0.1	20.8	0.1	1219	1	full
5	101.6	0.1	10.40	0.08	1016	1	full
14	76.2	0.1	7.62	0.03	762.0	0.8	full
8	50.825	0.013	5.197	0.025	304.8	0.8	full
4	50.825	0.005	5.197	0.013	304.8	0.8	full
3	50.825	0.005	2.718	0.005	304.8	0.8	half
12	50.80	0.05	5.197	0.013	457.2	0.8	full
2	25.425	0.005	2.596	0.005	304.8	0.8	full
1	25.425	0.005	1.359	0.005	304.8	0.8	half
15	25.40	0.05	2.596	0.013	457.2	0.8	full
10	25.40	0.05	2.596	0.013	304.8	0.8	full
11	19.1	0.1	1.946	0.013	229	1	full
7	12.7	0.1	1.359	0.051	152	1	full
9	9.58	0.05	0.889	0.051	152	1	full
13	6.35	0.05	0.6350	0.0127	152	1	full

Figure 2a. Cylinder set-up showing the robust frame construction. The PDV probes sit inside the eight aluminum rectangular solids. The detonation goes upwards.

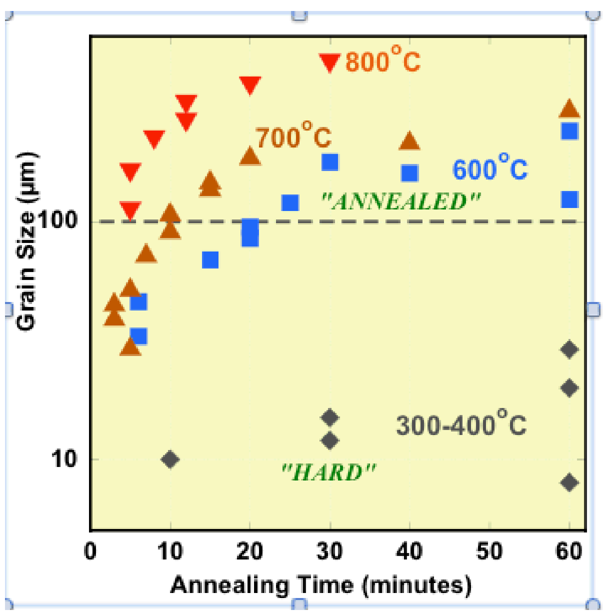

Figure 2c. Summary of annealing and grain size for OFHC copper [3]. Other 600°C data disagrees with these results so that 700°C is probably the temperature to shoot for.

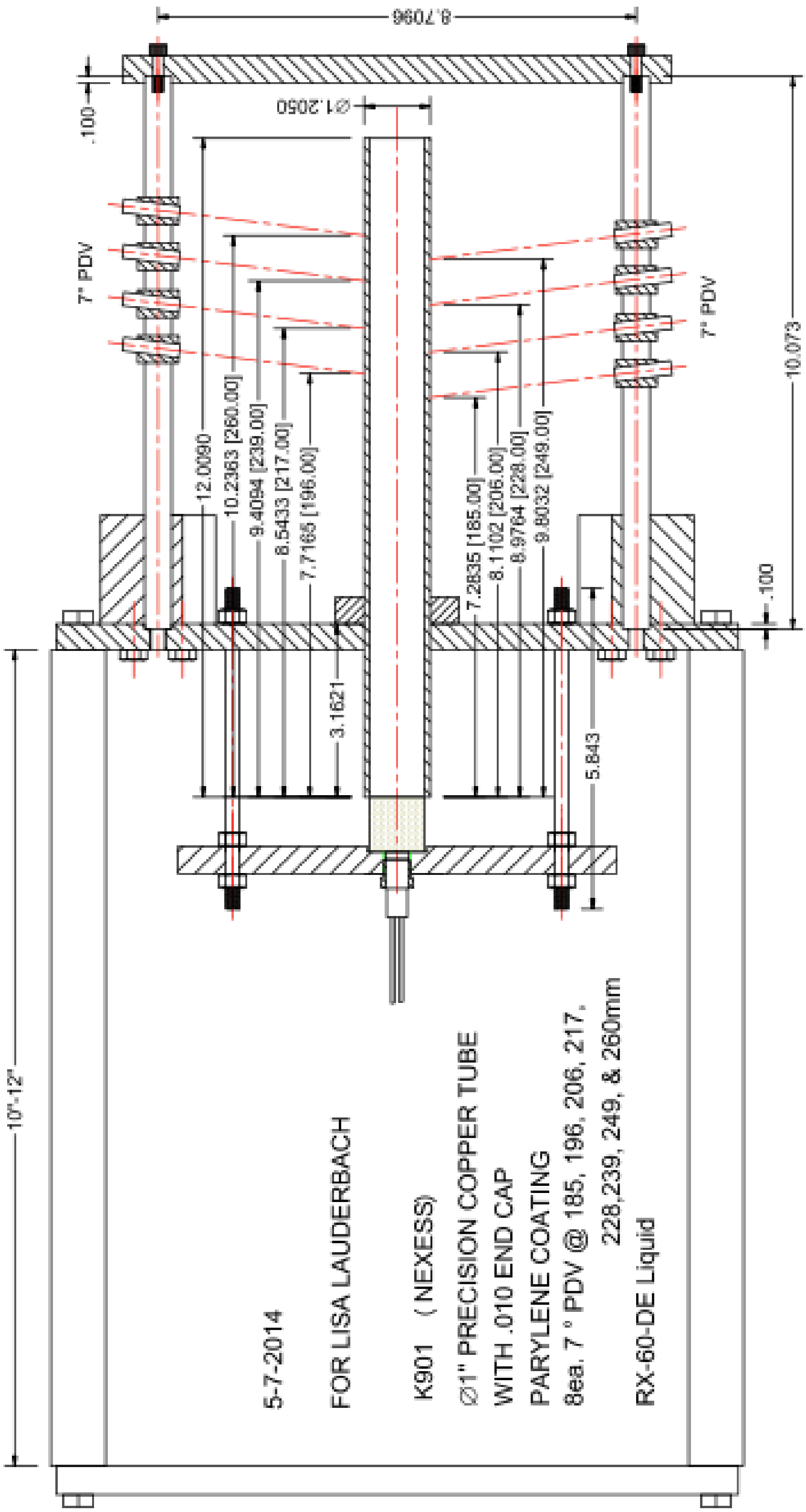

Figure 2b. Diagram for the Cylinder test shown in Figure 2a.

The explosive in a Cylinder test is always made of short pieces, maybe 1 inch long from a ram-press and maybe 2 to 6 inches long from an isostatic pressing. We want to keep the ends as flat as possible so that the air gap is small between adjacent parts, which are usually stacked vertically so that gravity holds them down. The pins and probes should be placed so that they fall between the gaps. More important yet is to keep the radial air gaps between the explosive and the copper as small as possible, and this is best done by the lead experimentalist working with the part maker and the mechanical technician to get the best fit as the process goes on.

We may want to change the temperature for a Cylinder shot. In order to get the smallest air gap possible, we need to know the linear strains of the explosive and the copper, and these are listed in Table 2b [4,5], which, because of its length, is listed at the end of this section. The definitions of the directions are shown in Figure 2d. The strain is the length fraction that the part changes by, either swelling or shrinking because of the temperature change. All pressing of powdered explosives is asymmetric, and there always is one direction that is higher in strain and another that is lower. Table 2c summarizes the possibilities. For a ram-pressed cylinder of explosive, the single axial direction always has the high strain and the two sideways directions have the low strain. For a ram-pressed Cylinder test, the sideways strain is always used in calculating the fit at another temperature. The explosive may be isostatically-pressed and cut into a hemisphere with the asymmetry of the pressing process. The radial (of the hemisphere) direction always has a higher value than the two transverse directions. If a cylinder is cut from a hemisphere, It is necessary to know what direction the cylinder axis has relative to the hemisphere in order to decide on the strain.

There are two ways to get detonation velocities. If there are only two PDV probes or a streak camera, then two pin rings, with 6 pins each, can be placed on the last half of the cylinder. Each position vs. time pair is plotted and the gross outliers are thrown away. The standard deviation is obtained by comparing all the good points with the fitted value. The detonation velocity for a modern 6 to 8-probe PDV shot comes from the jump-off times of the PDV signals themselves. It is necessary to make a position-time linear fit, which gives the velocity and by comparison of the fit with the data, the standard deviation.

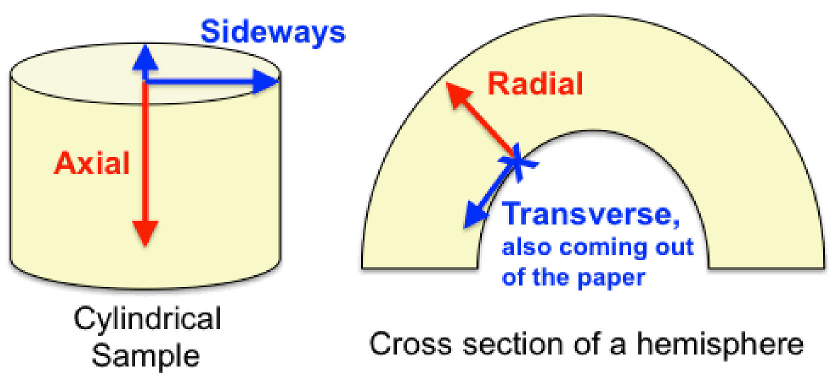

Figure 2d. Here are the definitions of strain: axial and sideways apply to a cylinder; radial and transverse apply to an isostatically-pressed hemisphere. The pressing process is always asymmetric.

Table 2c. The combinations of geometry that have high and low linear strains. The numbers indicate the degrees of freedom.

	HIGH	LOW
Ram-Pressed Cylinder	Axial-1	Sideways-2
Isostatically-Pressed Hemisphere	Radial-1	Transverse-2
Cyinder cut from Henisphere		
Axial alligned with Radial	Axial-1	Sideways-2
Axial alligned with Transverse	Sideways-2	Axial-1

Note in Figure 2b where the PDV probes are relative to the clamp and to the top end. We don't want them too close to the clamp or a plastic pin ring, which will outgas when shocked. At the top end, the PDV signals will die out too fast if the probe is too close to the end. With all PDV's and no pin rings, good data has been taken from 31 to 95% of the distance along the cylinder, although 50 to 85% is probably safer.

The data taken by PDV is good until it glitches, which is caused by the outer copper surface getting stretch marks as shown in Figure 2e. This usually starts at a relative volume of about 13 to 17.

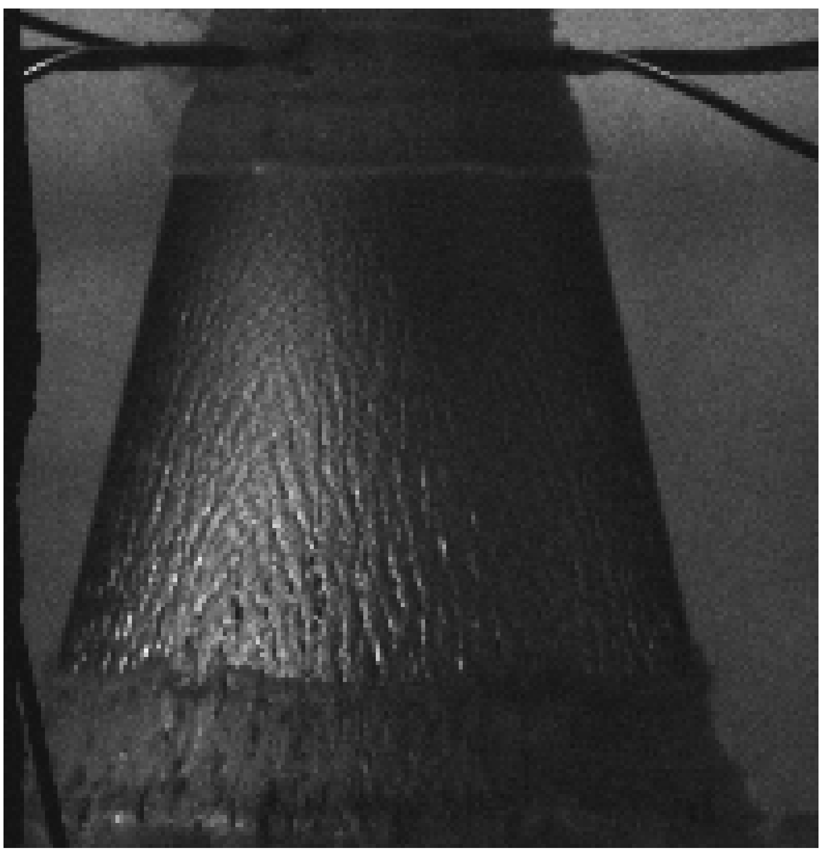

Figure 2e. Framing camera picture of an expanding un-annealed copper tube with stretch marks on the outside beginning at about v = 15 (taken by Lou Ferranti, Jr., LLNL).

Table 2b. List of averaged linear strains to be used for calculating thermal expansion.

Temp (°C)	LX-17 Density at 21°C (g/cc) 1.90	LX-17 Axial/Radial Linear Strain (dimension-less)	LX-17 Sideways/ Transverse Strain (dimension-less)	PBX 9502 Density at 21°C (g/cc) 1.89	PBX 9502 Axial/Radial Linear Strain (dimension-less)	PBX 9502 Sideways/ Transverse Strain (dimension-less)
-60	1.920	-4.0E-03	-3.2E-03	1.913	-4.8E-03	-3.5E-03
-55	1.919	-3.9E-03	-3.1E-03	1.911	-4.5E-03	-3.3E-03
-50	1.919	-3.8E-03	-3.0E-03	1.910	-4.2E-03	-3.1E-03
-40	1.917	-3.4E-03	-2.8E-03	1.907	-3.6E-03	-2.7E-03
-30	1.915	-3.1E-03	-2.5E-03	1.904	-3.0E-03	-2.3E-03
-20	1.913	-2.6E-03	-2.1E-03	1.902	-2.5E-03	-1.8E-03
-10	1.910	-2.1E-03	-1.7E-03	1.899	-1.9E-03	-1.4E-03
0	1.907	-1.5E-03	-1.2E-03	1.896	-1.3E-03	-9.6E-04
10	1.904	-8.3E-04	-6.6E-04	1.893	-7.1E-04	-5.1E-04
20	1.900	-7.9E-05	-6.3E-05	1.890	-6.7E-05	-4.8E-05
21	1.900	0.0E+00	0.0E+00	1.890	0.0E+00	0.0E+00
30	1.896	7.4E-04	5.9E-04	1.887	6.3E-04	4.5E-04
40	1.892	1.6E-03	1.3E-03	1.884	1.4E-03	9.8E-04
50	1.887	2.6E-03	2.1E-03	1.880	2.3E-03	1.6E-03
60	1.882	3.6E-03	2.9E-03	1.875	3.3E-03	2.2E-03
70	1.877	4.8E-03	3.8E-03	1.870	4.4E-03	3.0E-03
75	1.874	5.4E-03	4.3E-03	1.868	5.0E-03	3.4E-03
80	1.871	6.0E-03	4.7E-03	1.865	5.7E-03	3.9E-03

Temp (°C)	ufTATB Density at 21°C (g/cc) 1.80	ufTATB Axial/Radial Linear Strain (dimension-less)	ufTATB Sideways/ Transverse Strain (dimension-less)	LX-16 Density at 21°C (g/cc) 1.60	LX-16 Axial/Radial Linear Strain (dimension-less)	LX-16 Sideways/ Transverse Strain (dimension-less)
-60	1.825	-6.9E-03	-3.3E-03	1.624	-5.4E-03	-4.7E-03
-55	1.823	-6.5E-03	-3.1E-03	1.623	-5.1E-03	-4.4E-03
-50	1.822	-6.1E-03	-2.9E-03	1.621	-4.8E-03	-4.2E-03
-40	1.819	-5.4E-03	-2.4E-03	1.619	-4.2E-03	-3.7E-03
-30	1.816	-4.6E-03	-2.0E-03	1.616	-3.6E-03	-3.2E-03
-20	1.813	-3.8E-03	-1.6E-03	1.613	-2.9E-03	-2.6E-03
-10	1.810	-2.9E-03	-1.3E-03	1.610	-2.2E-03	-2.1E-03
0	1.807	-2.0E-03	-8.9E-04	1.607	-1.5E-03	-1.4E-03
10	1.804	-1.1E-03	-4.8E-04	1.604	-8.2E-04	-7.7E-04
20	1.800	-1.0E-04	-4.6E-05	1.600	-7.6E-05	-7.2E-05
21	1.800	0.0E+00	0.0E+00	1.600	0.0E+00	0.0E+00
30	1.797	9.7E-04	4.3E-04	1.597	6.9E-04	6.6E-04
40	1.793	2.1E-03	9.5E-04	1.593	1.5E-03	1.4E-03
50	1.789	3.3E-03	1.5E-03	1.589	2.3E-03	2.2E-03
60	1.784	4.7E-03	2.2E-03	1.585	3.1E-03	3.1E-03
70	1.779	6.1E-03	2.9E-03	1.581	4.0E-03	3.9E-03
75	1.776	6.8E-03	3.3E-03	1.579	4.4E-03	4.4E-03
80	1.773	7.6E-03	3.7E-03	1.577	4.9E-03	4.9E-03

Table 2b. Linear strain continued.

Temp (°C)	RX-55-AY Density at 21°C (g/cc) 1.82	RX-55-AY Axial/Radial Linear Strain (dimension-less)	RX-55-AY Sideways/ Transverse Strain (dimension-less)	LX-04 Density at 21°C (g/cc) 1.865	LX-04 Axial/Radial Linear Strain (dimension-less)	Copper Density at 21°C (g/cc) 8.93	Copper Isotropic Linear Strain (dimension-less)
-60	1.840	-3.9E-03	-3.4E-03	1.896	-6.9E-03	8.966	-1.3E-03
-55	1.839	-3.7E-03	-3.2E-03	1.895	-6.5E-03	8.963	-1.2E-03
-50	1.837	-3.5E-03	-3.0E-03	1.893	-6.2E-03	8.961	-1.2E-03
-40	1.835	-3.0E-03	-2.6E-03	1.890	-5.4E-03	8.957	-1.0E-03
-30	1.833	-2.5E-03	-2.2E-03	1.886	-4.7E-03	8.953	-8.4E-04
-20	1.830	-2.1E-03	-1.8E-03	1.882	-3.8E-03	8.948	-6.8E-04
-10	1.828	-1.6E-03	-1.3E-03	1.878	-3.0E-03	8.944	-5.1E-04
0	1.825	-1.1E-03	-9.0E-04	1.874	-2.1E-03	8.939	-3.5E-04
10	1.823	-5.9E-04	-4.7E-04	1.870	-1.1E-03	8.935	-1.8E-04
20	1.820	-5.4E-05	-4.3E-05	1.865	-1.0E-04	8.930	-1.7E-05
21	1.820	0.0E+00	0.0E+00	1.865	0.0E+00	8.930	0.0E+00
30	1.818	4.9E-04	3.9E-04	1.861	9.6E-04	8.926	1.5E-04
40	1.815	1.0E-03	8.2E-04	1.856	2.1E-03	8.921	3.2E-04
50	1.813	1.6E-03	1.2E-03	1.851	3.3E-03	8.917	4.9E-04
60	1.810	2.1E-03	1.7E-03	1.845	4.5E-03	8.912	6.6E-04
70	1.808	2.7E-03	2.1E-03	1.839	5.8E-03	8.908	8.3E-04
75	1.806	2.9E-03	2.3E-03	1.836	6.5E-03	8.906	9.2E-04
80	1.805	3.1E-03	2.5E-03	1.833	7.2E-03	8.903	1.0E-03

3. Analytic Model of Cylinder Energies

The best definition for the relative volume, v, appears to be

$$v \approx \left(\frac{S}{S_o}\right)^2 , \qquad (1)$$

where S_o is the initial scaled inner copper radius (always 12.7 mm) and S is the scaled inner copper radius at a later time. This is equivalent to just drawing a perpendicular line through the cylinder, squaring it for area and pretending it is a volume. It's just a thin mental "coin" sitting at a particular location. Figure 3a shows that the calculated contours are not straight lines. All this, however, affects the equation-of-state that will be made, not the detonation energy densities.

Table 3a lists the scaled displacements we measure, the approximate relative volume we use and the actual calculated relative volumes using Eq. 1. Full-wall is the standard copper wall thickness; half-wall is half as thick, with the wall 1/10th the radius. Before lasers came along, half-wall seemed a way of getting better resolution. Today, nobody would spend the money, but the old results have been very useful in working out the analytical model. In Table 3a, we see that the calculated relative volumes are different for the two types of tubes and change with relative volume. At some point, adding complication to the analytic model has to stop, and all modern tubes are all full-wall, so we use the rounded-off approximate values. The code calculations are insensitive to small changes in v and we don't have a way of defining it for certain, anyway.

Figure 3a shows calculated relative volumes for four cases as compared with the sample model. The calculated values wander about but usually aren't far from the model.

Table 3a. Calculated relative volumes for two different copper cylinder sizes.

Scaled Displacement (mm)	Approx. Relative Volume	Relative Volume Full Wall	Relative Volume Half Wall
2.5	1.5	1.51	1.47
6.0	2.4	2.36	2.26
12.5	4.4	4.33	4.13
19.0	7.0	6.83	6.53
25.5	10.0	9.85	9.45
32.0	13.5	13.40	12.89

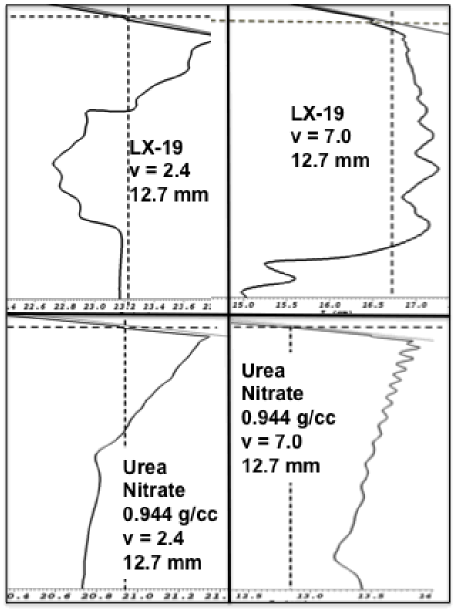

Figure 3a**.** Calculated contours for v = 2.4 and 7.0 for two explosives. The vertical dashed lines show where the slices are expected using Eq. 1. The X-axis is distance down the cylinder and the Y-axis is the radius of the explosive, with the axis at the bottom and the copper at the top.

We next show the final equations [6], then discuss each part. For PDV [7] and Fabry-Perot interferometry [8], we have

$$E_d(laser) = \overset{\text{Air Gap}}{g}\left(\left(\overbrace{\rho_m\left(\frac{S+X}{S_o}\right)^2 \ln\left(\frac{S+X}{S}\right) + \frac{\rho_o}{4}\left(\frac{S+X}{S}\right)^2}^{\text{Wall Thinning}}\right)\left(\frac{\overset{\text{Velocity}}{u_\alpha}}{\underset{\text{Wall Tilt}}{\cos\Theta}}\right)^2 + \overset{\text{Work Hardening}}{E_{strain}} + \underset{\text{Heat Loss}}{E_{heat}} + \overset{\text{Spall}}{E_{spall}}\right) \tag{2}$$

and for the streak camera

$$E_d(streak) = \overset{\text{Air Gap}}{g}\left(\left(\overbrace{\rho_m\left(\frac{S+X}{S_o}\right)^2 \ln\left(\frac{S+X}{S}\right) + \frac{\rho_o}{4}\left(\frac{S+X}{S}\right)^2}^{\text{Wall Thinning}}\right)\overset{\text{Velocity}}{u_o^2} + \underset{\text{Work Hardening}}{E_{strain}} + \overset{\text{Heat Loss}}{E_{heat}} + \overset{\text{Spall}}{E_{spall}}\right). \tag{3}$$

The two descriptions include u_o as the measured outer wall velocity of the streak camera and u_α the laser-measured (PDV or Fabry-Perot interferometry), The angle Θ describes the tilt of the wall.

The effect of making all these corrections is considerable, as shown in Table 3b. Many people continue to use the old Gurney energy, which is clearly too low. The wall thinning is the most important correction, with the air gap and work hardening next. Heat loss and spall are small corrections.

The analytical model has been extensively tested against the LLNL production code and is in agreement, excepting that the code does not have a spall or irreversible heat model, which are small corrections. The overall agreement is within the estimated code-running error of ±0.1 k/cc or ±0.001 Mb, which is obtained by careful repetititve runs.

We may summarize in Table 3c by considering various corrections for an ideal explosive with $E_d(2.4)$ of 0.0700 Mb. We used three metal models plus a spall model that requires 200 zones/cm and find all of them are different by the amount of uncertainty in running the code. The default model is always Steinberg-Guinan with no spall.

Table 3b. Corrections to energy density in a 1.63 g/cc PBX 9407 Cylinder test.

Explosive	Energy Input	$E_d(2.4)$ (kJ/cc)	$E_d(4.4)$ (kJ/cc)	$E_d(7.0)$ (kJ/cc)
PBX 9407	Gurney	2.94	3.50	3.79
1.631 g/cc	wall thinning	2.54	2.78	2.89
	air gap	0.11	0.10	0.10
	work hardening	0.13	0.21	0.30
	heat	0.03	0.03	0.03
	spall	0.04	0.04	0.04
	sum	5.79	6.66	7.15

Table 3c. Errors in running the computer model on copper.

Effect	(kJ/cc)	(Mb)
No heat loss and spall	+0.10	+0.0010
Use the PTW model	-0.10	-0.0010
Use the MTS model	+0.15	+0.0015
Use Johnson spall	-0.10	-0.0010
Code-running error	±0.10	±0.0010

All the errors are comparable in size and many must cancel out, but it means that an error band of at least ±2% probably exists for the absolute value of the energy density. Most computer studies concentrate on precision, where a small change in a variable can easily be seen but the absolute value is poorly known. Another important issue is the error of running a computer model, which incorporates human factors, inherent code jitter and the constant rewriting of the code.

My error bars for code-running assume a careful job where particular relative volume points are studied, not just eyeball comparisons of curves. It also assumes that the same problem is run several times at different sittings over 1 to 2 years.

Archiving the data is important. Table 3d shows a piece of the permanent Cylinder test database for the explosive EGDN. On the first line, we next list the density, shot number, type of measurement (PDV, Fabry-Perot or streak camera), the angle of the probe to the cylinder, the detonation velocity, outer explosive radius, inner copper radius and wall thickness. The scale factor is the inner copper radius in inches. It is also the number we divide by to convert to scaled times or distances. Starting the second line is the viewing position along the cylinder with zero being the detonator end; then comes the overall cylinder length. The final data in the second section are the measured velocities; first jump off, then the values at 2.5, 6.0, 12.5, 19, 25.5 and 32 scaled-mm of wall displacement. At the bottom are the corresponding detonation energy densities for all the values except jumpoff. The approximate values of the relative volumes, v, are listed. All this is what the analytical model does for us. In making a JWL with our Tweaker3 program, we need three points on the adiabat to define the curve, and we use v = 2.4, 4.4 and 7.0, which correspond to the scaled displacements of 6, 12.5 and 19 mm.

Table 3d. Data entry for EGDN with all the input quantities, the measured copper wall velocities and the calculated detonation energy densities. The logic for the calculations would lie on the spreadsheet to the right.

Explosive	Expl. Density (g/cc)	Shot No.	Type	An-gle (deg)	Detvel (mm/μs)	Radius Outer HE (mm)
EGDN, probe 1	1.492	869	PDV	7	7.383	12.717
EGDN, probe 2	1.492	869	PDV	7	7.383	12.717
EGDN, probe 3	1.492	869	PDV	7	7.383	12.717
EGDN, probe 4	1.492	869	PDV	7	7.383	12.717
Average EDGN	1.492				7.383	

	Radius Inner Metal (mm)	Wall Thick (mm)	Scale factor	scaled wall thick	View Position (mm)	Cyl Length (mm)
EGDN, probe 1	12.717	2.591	1.0013	2.587	186	305
EGDN, probe 2	12.717	2.591	1.0013	2.587	209	305
EGDN, probe 3	12.717	2.591	1.0013	2.587	232	305
EGDN, probe 4	12.717	2.591	1.0013	2.587	256	305

	Measured Wall Velocity (mm/μs) at these Scaled Outer Wall Displacements (mm)						
	jumpoff	2.5	6	12.5	19	25.5	32
EGDN, probe 1	0.597	1.108	1.310	1.476	1.564	1.607	1.632
EGDN, probe 2	0.595	1.116	1.307	1.477	1.552	1.598	1.628
EGDN, probe 3	0.599	1.111	1.311	1.482	1.557	1.600	1.631
EGDN, probe 4	0.587	1.123	1.312	1.481	1.556	1.594	1.630
Average EDGN	0.595	1.114	1.310	1.479	1.557	1.600	1.630
Stdev	0.005	0.007	0.002	0.003	0.005	0.005	0.002

A common practice is to use only the 1943 Gurney equation to calculate the detonation energy density, E_d [9]. It is usually written as

$$E_d = \left(\frac{M}{C} + \frac{1}{2}\right)\frac{u^2}{2}, \quad (4)$$

where M is the mass of metal per unit length, C the mass of explosive and u the wall velocity.

In our terminology, at a given relative volume, v, this is

$$E_d = \left\{\frac{\rho_m}{\rho_o}\left(\frac{(S_o + X_o)^2 - S_o^2}{S_o^2}\right) + \frac{1}{2}\right\}u_o^2 \quad (5)$$

where ρ_m and ρ_o are the initial copper and explosive densities, S_o is the scaled inner radius (always 12.7 mm), X_o the scaled wall thickness and u_o is the measured wall velocity perpendicular to the axis, as is the case with a streak camera.

Eq. 4/5 assumes the same wall thickness always, which can't be right, so the first correction is for wall-thinning [10]

$$E_d = \left(\rho_m\left(\frac{S+X}{S_o}\right)^2 \ln\left(\frac{S+X}{S}\right) + \frac{\rho_o}{4}\left(\frac{S+X}{S}\right)^2\right)u_o^2, \quad (6)$$

where S and X are the inner radius and wall thickness at a later time during expansion. We have moved away from using only initial quantities. This is a good equation to use as a general equation that gets most of the energy without having to worry about the small corrections.

This is the first step beyond the simple Gurney model, and the result is the basic equation used in analyzing Cylinder test data. Both assume the cylinder is expanding everywhere at the same rate; there is no detonation velocity or moving front. All dimensions are scaled to the 1-inch explosive diameter. We have: ρ_o = initial explosive density, ρ = later explosive density, ρ_m = initial copper density, S_o = initial explosive radius (always12.7 mm), X_o = initial copper thickness, S = later explosive radius, X = later copper thickness, u = copper velocity along the normal.

Metal Section. The scaled outer radius is determined using

$$S + X = S_o + X_o + d, \quad (7)$$

where d is the scaled displacement of 6, 12.5 or 19 mm and S_o is always 12.7 mm. If the cylinder stays the same, the copper is conserved if

$$(S + X)^2 - S^2 = (S_o + X_o)^2 - S_o^2, \quad (8)$$

We have

$$S=\left\{(S+X)^2+\left[S_o^2-(S_o+X_o)^2\right]\right\}^{1/2}. \qquad (9)$$

To resume the derivation, we solve Eq. 8 for $(S+X)^2$

$$(S+X)^2=S^2+\left[(S_o+X_o)^2-S_o^2\right]. \qquad (10)$$

We differentiate to get

$$2(S+X)\frac{d(S+X)}{dt}=2(S+X)u=2S\frac{dS}{dt} \qquad (11)$$

so that at the inner wall at S

$$u_s=\frac{dS}{dt}=\left(\frac{S+X}{S}\right)u. \qquad (12)$$

We want to integrate through the copper from S to S+X using the scaled radial variable r, where we define a linear velocity function

$$u(r)=\left(\frac{S+X}{r}\right)u. \qquad (13)$$

We shall convert the energy in the wall to a copper energy density, E_w, by dividing by πS_o^2, the radial "volume".

$$E_w=\frac{\rho_m}{2\pi S_o^2}\int_S^{S+X}2\pi r\left(\frac{S+X}{r}u\right)^2 dr=\frac{\rho_m u^2(S+X)^2}{S_o^2}\int_S^{S+X}\frac{dr}{r}, \qquad (14)$$

where E_W is the energy in the copper. We get

$$E_w=\frac{\rho_m u^2(S+X)^2}{S_o^2}\ln\left(\frac{S+X}{S}\right). \qquad (15)$$

2. Explosive/Gas Section. We can use Eq. 13 at S also for the outer edge of the gas, and we assume that the radial velocity is proportional to the radius

$$u(r) = \frac{r}{S} u. \tag{16}$$

But Eq. 13 also describes u(r). We combine the two equations to get

$$u(r) = \frac{S+X}{S^2} ru. \tag{17}$$

We integrate the variable r from 0 to to S in the gas. The energy density in the gas, E_g, is

$$E_g = \frac{\rho}{2\pi S_o^2} \int_0^S 2\pi r \left[\left(\frac{S+X}{S^2} \right) ru \right]^2 dr. \tag{18}$$

This contains the later density of the gas, ρ, which we want to convert to the initial one, using

$$\pi \rho S^2 = \pi \rho_o S_o^2 . \tag{19}$$

and obtain

$$E_g = \frac{\rho_o}{S^2} \frac{(S+X)^2}{S^4} u^2 \int_0^S r^3 \, dr = \frac{\rho_o}{4} \frac{(S+X)^2}{S^2} u^2. \tag{20}$$

We combine all terms and we finally get

$$E_d = \left\{ \rho_m \left(\frac{S+X}{S_o} \right)^2 \ln \left(\frac{S+X}{S} \right) + \frac{\rho_o}{4} \left(\frac{S+X}{S} \right)^2 \right\} u^2. \tag{21}$$

The PDV or Fabry-Perot bean looks in at some angle and sees the Doppler velocity of the moving wall. The streak camera sits at 0^o and sees the wall move past it. How do we resolve these differences [11-12]?

To answer this, the model we use assumes that the copper wall folds back like a rigid "door" with the detonation energy quickly moving from the inside to the outside wall. The schematic defining the angles is shown in Figure 3b. At the bottom is the outer copper wall, now bent at time t at an angle Θ to the cylinder axis. The vector u_m is perpendicular to the wall with the angle Θ, referenced to the perpendicular to the initial wall. The vector u_β is the actual metal particle velocity at the angle β. The PDV probe looks in at the angle α, which has been set by various researchers at 4-10^o and by us to 7^o. The probe vector u_α is the Doppler velocity as seen at the angle α, i.e. the projection of u_β on □$_\alpha$. The probe angle, α, is set close to β so that the two are essentially the same. Real streak camera data is only taken at 0^o along the vector u_o.

This vector is not a Doppler velocity but is phase or laser-spot moving velocity determined by differentiating distance and time along the path. Finally, the vectors xdot and ydot are components of u_β, and they can be estimated by from code runs. From Figure 3b, we see these relations.

$$\sin\Theta = \frac{u_m}{U_s} \tag{22}$$

$$\tan\Theta = \frac{u_o}{U_s} \tag{23}$$

$$\cos(\beta - \alpha) = \frac{u_\alpha}{u_\beta} \tag{24}$$

$$\tan\beta = \frac{xdot}{ydot} \tag{25}$$

$$\cos(\Theta - \beta) = \frac{u_m}{u_\beta} \tag{26}$$

$$\cos\Theta = \frac{u_m}{u_o} \tag{27}$$

We have differentiated between the measurement direction, the copper direction of motion and the perpendicular to the wall. We also distinguish between the component of velocity and the motion of the laser spot, which is the phase velocity. Eq. 23 is the equation for the streak camera, and the angle Θ is easily defined in this case.

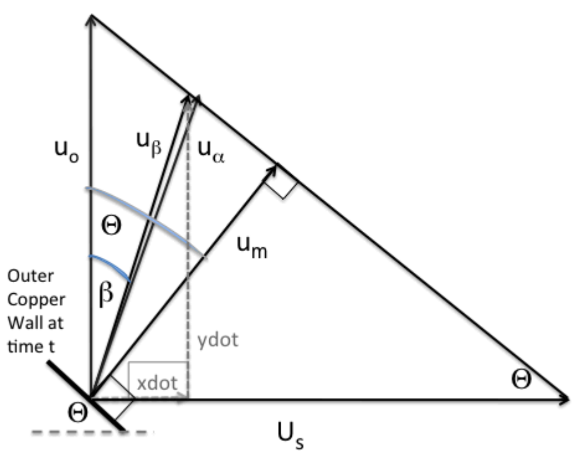

Figure 3b. Schematic of the titled copper cylinder wall at time t with the various velocity vectors and angles. All the activity is outside the copper wall. The angles α and β are about the same.

$$\tan\Theta = \frac{u_o}{U_s} \tag{28}$$

for the streak camera. For the PDV and Fabry, we use Eqs. 22, 24 and 26 to get

$$\frac{u_\alpha}{U_s} = \frac{\cos(\beta - \alpha)\sin\Theta}{\cos(\Theta - \beta)} \approx \sin\Theta, \tag{29}$$

which is transcendental. Very roughly, in order to get a quick result

$$\frac{u_\alpha}{U_s} \approx \sin\Theta. \tag{30}$$

From the above set of angles, we take

$$u_\alpha = u_\beta \cos(\beta - \alpha) \tag{31}$$

$$u_\beta = \frac{u_m}{\cos(\Theta - \beta)} \tag{32}$$

$$u_m = u_o \cos\Theta. \tag{33}$$

We combine these to get

$$\frac{u_o}{u_\alpha} \approx \left[\frac{\cos(\beta)}{\cos(\beta - \alpha)\cos\Theta}\right] \approx \frac{1}{\cos\Theta}. \tag{34}$$

Using the half-angle approximation below, we get

$$\frac{u_o}{u_\alpha} \approx \left[\frac{\cos(\Theta/2)}{\cos(\Theta/2 - \alpha)\cos\Theta}\right] \approx \frac{1}{\cos\Theta}. \tag{35}$$

For a typical full-wall angle of Θ = 12^{o}, we get

$$\frac{u_\alpha}{u_o} = 0.984, \tag{36}$$

which agrees with the measured Fabry/streak camera ratios taken ten years ago.

The angle of tilt of the copper wall is

$$\Theta(laser) = \sin^{-1}\left(\frac{u_\alpha}{U_s}\right) \tag{37}$$

$$\Theta(streak) = tan^{-1}\left(\frac{u_o}{U_s}\right). \tag{38}$$

We take the displacement at the same distances (6, 12.5 and 19 scaled mm) for streak and laser, but they are not really the same thing. The measured outer wall displacement, d, is straight-forward for the streak camera. For the laser, we are following a curved track described with the hinged door model. The “door” track may be mentally straightened using the partlcle velocity angle, so that

$$d(laser) \approx \frac{d(streak)}{\cos\beta} \approx \frac{d(streak)}{\cos(\Theta/2)}. \quad (39)$$

This is a small difference and the wall velocity changes slowly with d at v = 2.4 and beyond, so we have ignored this issue.

The Half Angle Model for the Particle Velocity Vector [13]

We don't know what the particle velocity angle β is. Pictures show that the wall looks fairly straight with only a slight bend when it first starts. We assume that the copper wall is flat and rigid and moves outward always at an angle Θ as shown in Figure 3c for the inside of the cylinder. We can think of the wall as having rotated on a hinge upward around point O. The particle velocity vector then moves along the path AB in expansion. There are two isosceles triangles inside ABO with angles $\Theta/2$, which tell us that AB is at $\Theta/2$ to the perpendicular, so that

$$\beta \approx \Theta/2. \quad (40)$$

All pressed solid explosives do not perfectly fit into the copper tubes and there is an air gap, which must cause a loss of energy to the wall [3]. The scaled gap width is

$$X_{gap} = \frac{inner\ copper\ radius - outer\ explosive\ radius}{scale\ factor}. \quad (41)$$

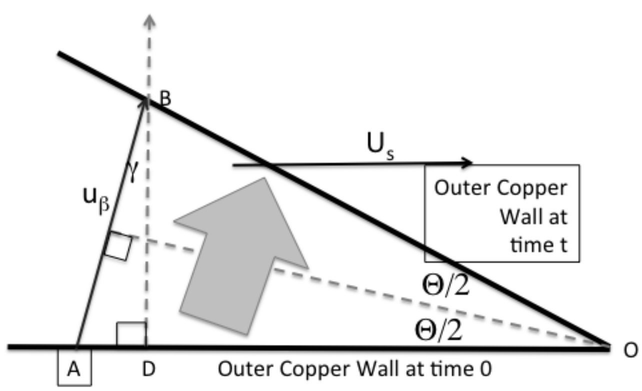

Figure 3c. Derivation of the half-angle approximation with everything inside the copper wall. Only the particle velocity vector, u_β, is shown. The wall moves up as though it rotated on a hinge about point O.

Old cylinder shots had scaled gaps of averaging 0.04 mm, whereas good modern shots can be reduced to 0.01 mm. We have modeled Cylinder tests of different explosives using a CALE-like Lagrange finite-element code with partial Eulerian relaxation to offset zone tangling. Programmed burn was used as the explosive model with square zoning at 8 zones/mm. A special package gave either the copper particle velocity as seen at 7^{o} by PDV or the 0^{o} phase velocity as seen by the streak camera.

For the air gap between the explosive and the inner copper wall, we modeled PBX 9501, LX-17, potassium chlorate 80/sugar at 1.04 g/cc and urea nitrate at 0.944 g/cc. The air gap energy multiplier, g, is determined from

$$g = \left[\frac{u(gap = 0)}{u(gapX)} \right]^2 \tag{42}$$

The multiplier increases linearly with increasing air gap width. The differences between explosives are not related to detonation velocity but to the tilt angle Θ.. We find this fit to the calculations

$$g = 1 + 170 \frac{X_{gap}}{\Theta^{2.6}}, \tag{43}$$

where X_{gap} is the scaled air gap, which can range from 0 to 0.3 mm in Eq. 42. This effect makes liquid and powdered explosives special because they have no air gap. The effect of air gaps can be 1-2% with the effect being worst for cold samples, which shrink more.

We move on to mechanisms that cause lost energy in the copper. The overall energy density lost in the copper is related to the energy density lost in the explosive by this

$$E_d(\text{explosive}) = \left[\frac{S_o^2}{S_o^2 + X_o^2} \right] E_d(metal), \tag{44}$$

where S_o is the initial inner cylinder radius and X_o is the initial cylinder wall thickness. Eq. 44 simply makes a volume correction of 0.45 for full-wall and 0.22 for half-wall, which finally explains the difference.

We ran the Cyinder test in the code at 80 z/cm with various explosives and measured the various properties in the copper wall. These include the maximum shock pressure on the inside copper wall, P_{Cu}, the first three ringing relative volume minima with the first being the lowest, and the average strains for the explosive at relative volumes of 2.4, 4.4 and 7.0. We relate the initial shock pressure to the detonation velocity of the explosive used to produce it by

$$U_s(mm/\mu s) = 4.288 + 0.1817 P_{Cu}(GPa). \tag{45}$$

Using the detonation velocity is a more convenient way to calculate properties for the hundreds of Cylinder tests than shock pressure, which we rarely know. The largest remaining issue present in the codes is copper work hardening [6], where our code uses the Steinberg-Guinan (S-G) model, which was created for shock wave work in the region 1 to 60 GPa [14, 15]. Its simplicity allows us to calculate an analytic solution, The S-G model is given by

$$Y = Y_o\left(1+\beta\varepsilon\right)^n \frac{G}{G_o} < Y_{\max}, \tag{46}$$

where Y is the yield/shear/flow stress at some shear strain ε, Y_o is the yield stress at the start, β and n are coefficients, and G and G_o are the shear moduli at ε and initially. Y_{max} is the ultimate yield strength, which is never reached in most explosive problems. However, McQueen measured a value of 12-15 GPa at 40-57 GPa shock pressures as compared with Steinberg's 0.64 GPa, so that a larger number is appropriate [16]. Both Y and G stay always at the highest values they attain.

Eq. 46 is easy to convert to energy density due to work hardening in the metal by integrating with respect to strain

$$E_{strain}(metal) = \frac{Y_o}{\beta}\frac{G}{G_o}\frac{\left[1+\beta\varepsilon\right]^{n+1}}{n+1} \tag{47}$$

The shear modulus ratio comes from the measured data of Hayes [17]. For copper pressures, P_{Cu}, in the copper up to 55 GPa, we have

$$\frac{G}{G_o} \approx 1 + 0.0284 P_{Cu} \tag{48}$$

where the coefficient has a $\pm$20% error. We ran various explosives in the codes to get a conversion between shock pressure in the copper and the detonation velocity, U_s, of the explosive that caused it. The most useful equations are

$$\frac{G}{G_o} \approx 1,\ \ U_s < 3.8\ \ mm/\mu s. \tag{49}$$

$$\frac{G}{G_o} \approx 0.476 + 0.125 U_s,\ \ U_s > 3.8\ \ mm/\mu s. \tag{50}$$

For EGDN, we calcuate 1.43 whereas trying to reproduce the temperature in the actual S-G code model gives 1.38.

The strain is approximately given by the geometric relation involving outer radii

$$\varepsilon(simple) \approx \frac{(S+X)-(S_o+X_o)}{(S_o+X_o)}, \tag{51}$$

which is larger than 1 by v = 7. From running the codes, we determined an instantaneous strain, given by

$$\varepsilon \approx K U_s^k, \tag{52}$$

U_S, the detonation velocity, is used because that is readily available across all our shots. The coefficients are listed in Table 3e.

How sure are we about the strength of work hardening in copper? In Figure 3d, we show two shocked results in our range of 10^5 to 10^6 s^{-1}. The Tong annealed data [18] was taken on unusually thin samples. The Chhabildas data [19] was taken on 5 µm copper with the Huang and Asay double pulse method, used first on aluminum [20-22]. The analytic model they used appears to be controversial and it certainly leads to very high pressures, so that we are unsure of this data. We now turn to the electromagnetic expanding ring work of Gourdin [23, 24], who did both annealed copper at 150-200 µm and half-hard copper at 10 µm, but at low strain rates of 10^3 to 10^4 s^{-1}. At our laboratory, there is a bias toward using this kind of data because all quantities are well-known, but the less well-characterized shock wave work all suggests that the yield stresses will be higher. We next go to the yield stress vs. strain rate curves, admittedly not of high accuracy, and obtain a multiplication factor of 1.1 to 1.4 going from 10^3 to 10^5 s^{-1} and 1.7 to 1.9 from 10^4 to 10^6 s^{-1} [25, 26]. The increase with rate means that the slope of the curve will increase with rate. We use this to compare S-G curves at 25 GPa

Table 3e. Coefficients for calculating the instantaneous strain in copper at various relative volumes, v.

v	K	k
1.0	0.10	0.10
1.5	0.16	0.30
2.4	0.22	0.50
4.4	0.46	0.30
7.0	0.69	0.23
10.0	0.90	0.18
13.5	1.15	0.15

(like HMX) and 5 GPa (like Kinepak) with Gourdin's 10 µm data. This approach accepts Steinberg's assignment of his numbers literally as being for half-hard copper only. We then repeat the process with Gourdin's 150-200 µm data to estimate annealed copper. We find that we have to lower Y_o, the initial flow stress, from 0.12 GPa for half-hard to 0.10 GPa (0.0012 Mb) for annealed copper. Steinberg probably took a low-rate curve and moved it upward while fitting the initial jump of gun-shocked metals [14-15]. These would have had a strain of about 0.2-0.3 and our maximum is four times higher.

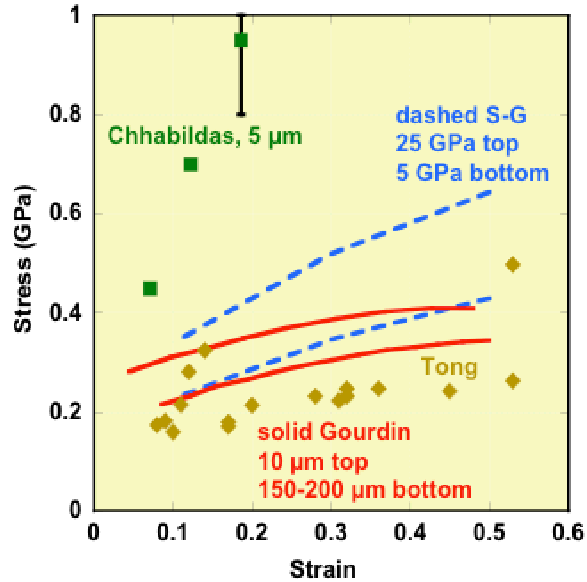

Figure 3d. Stress-strain data for copper. Chhabildas and Tong have shocked data, Gourdin's expanding ring, adjusted upward for strain rate, is set to agree with the Steinberg-Guinan model.

In the code, the JWL equations-of-state are changed over and over until a good fit to the wall velocities at the three standard positions is obtained. The code-running error we estimate to be $\pm$0.1 kJ/cc (0.0010 Mb).

Another error in the copper treatment is the irreversible loss of heat, which does not appear in the code. We use the Mie-Gruneison pressure equation-of-state [27], which Banerjee says should work to a copper relative volume of 0.8 [28], well below the Cylinder test minimum of 0.88 for calculated super-powerful CL-20. The energy density in the copper of the lost heat, E_{heat}, is given by [29]

$$E_{heat}(copper) = \frac{1}{2} P_{Cu}\left(1 - v_{Cu}\right) - \int_{v}^{1} P_{Cu}\, dv_{Cu} \tag{53}$$

where P_{Cu} is the Mie-Gruneison pressure. This is the smallest correction, being only 0.11 kJ /cc for CL-20, 0.04 kJ/cc for EGDN and zero for 1 g/cc explosives. Even the CL-20 value is about the size of the error of running the code. The energy equations are:

$$E_{heat}(kJ/cc) = 0, \quad U_s < 6.4 \ \ mm/\mu s. \tag{54}$$

$$E_{heat}(kJ/cc) \approx -0.264 + 0.0415 U_s, \quad U_s > 6.4 \ \ mm/\mu s. \tag{55}$$

Another error is spall in the copper, which also does not appear in our code. Spall is a spiltting of the copper wall into two radial pieces as a result of extreme tension in the metal. In Figure 3e, the low pressure potassium perchlorate

90/dodecane shows no spall. Both of the high pressure PETN show effects, with the lagging one clearly showing the first plateau delay charactistic of spall. LX-17, with a higher pressure, always shows glitches and delays.

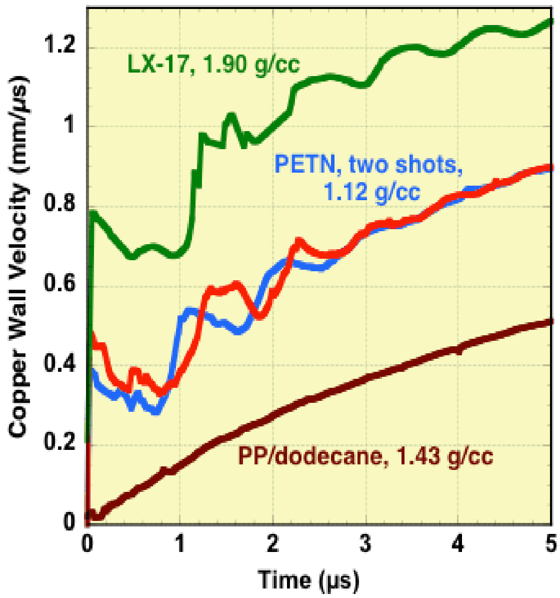

Figure 3e. Three cylinders wall velocities with descending pressures going top to bottom. The top two show spall; the bottom one does not.

We might expect that the delayed time to cross the first plateau would correlate with the measured wall velocities, but, as seen in Figure 3f, they do not. We take this as a first sign that the average energy density lost to spall, despite the observed glitches, is small, ie about 0.1 kJ/cc, which is our estimate of the code-running error.

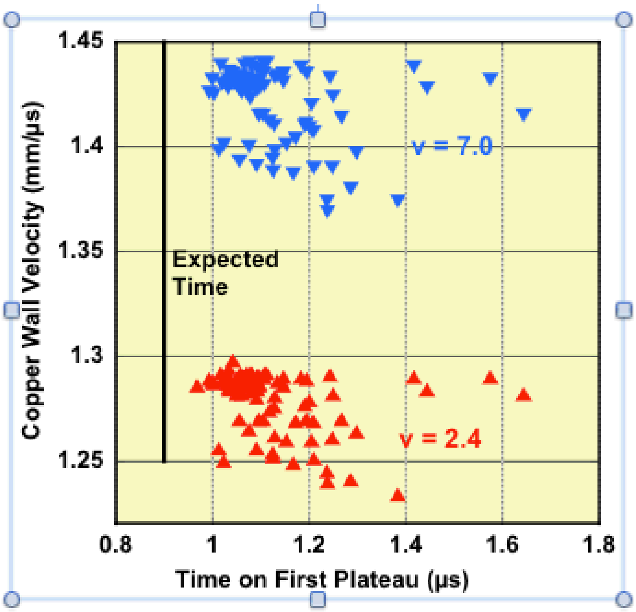

Figure 3f. The copper wall velocity shows no correlation with the first plateau crossing time for all LX-17 cylinder shots. This means that spall is small in the Cylinder test.

Luckily, copper calibration samples were shot in vacuum by Minich et. al. on a two-stage gas gun [30]. The copper flyer had a 17.5 mm radius and a 1.5 mm thickness; the target had a 12.5 mm radius and a 5 mm thickness. The dimensions were closen so that the time-to-rarifaction was about the same, with the side rarefaction coming sooner. The outer target face velocity was measured on-axis using VISAR. OFHC copper targets of multigrain copper were annealed to average grain sizes of 133 and 50 μm, which roughly correspond to our annealed copper. The detailed gunshot data for the multigrain samples is listed in Table 3f. The shock pressure is calculated by the impedance method

$$P_{Cu} = \rho_m \left(C_m + \frac{S_{1m} u_{flyer}}{2} \right) \frac{u_{flyer}}{2} . \tag{56}$$

Figure 3g shows a typical velocity trace. As expected, we have the same velocities

$$u_{flyer} \approx u_{start} . \tag{57}$$

The expected time for the side rarefaction to appear in shot 854 is 2.9 μs, based on the flyer velocity. The actual trace length without any major dropoff is 4.7 μs, which shows that the damage is so extensive as to greatly reduce the reshocked particle velocity.

Table 3f. Minich copper gunshot data used for heat/spall calibration.

Grain Size (μm)	Shot No.	Flyer velocity (mm/μs)	Target Jumpoff Velocity (mm/μs)	Later Target Velocity (mm/μs)	Impact Shock Pressure (GPa)	Energy Density Diff- (kJ/cc)	Spall Energy Density (kJ/cc)
133	847	1.898	1.82	1.75	45.4	1.15	0.75
	845	1.882	1.84	1.76	44.9	1.30	0.91
	843	1.625	1.62	1.56	37.4	0.82	0.52
	884	1.030	1.015	0.96	21.6	0.49	0.37
	812	0.828	0.834	0.79	16.8	0.33	0.25
	813	0.828	0.828	0.79	16.8	0.29	0.21
	807	0.724	0.715	0.68	14.5	0.25	0.20
	806	0.720	0.732	0.69	14.4	0.26	0.21
	808	0.567	0.562	0.53	11.0	0.17	0.15
	809	0.560	0.556	0.53	10.9	0.14	0.12
	810	0.323	0.317	0.29	6.0	0.08	0.07
50	868	1.928	1.93	1.86	46.3	1.18	0.78
	877	1.430	1.44	1.37	32.0	0.85	0.62
	876	1.170	1.16	1.10	25.1	0.60	0.43
	854	0.610	0.604	0.56	12.0	0.23	0.20
	855	0.310	0.305	0.27	5.8	0.09	0.08

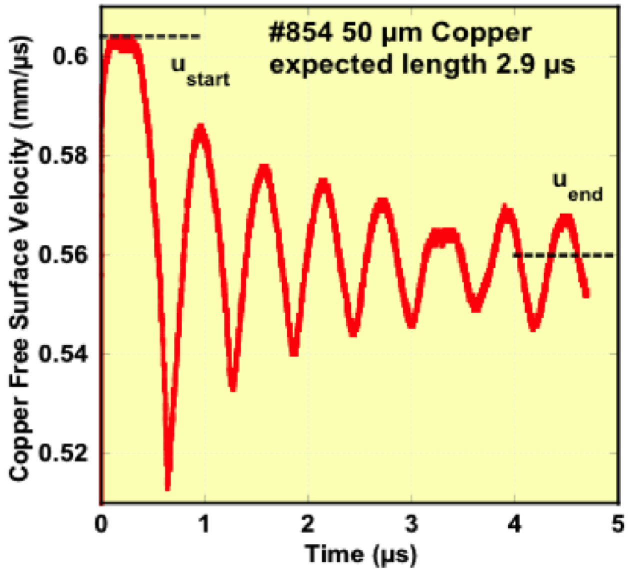

Figure 3g. Typical trace from the copper gun shot experiments. The difference-squared between the two velocities is a measure of the total energy density lost in the copper.

Curran appears to have been the first to notice that the free surface velocity of an aluminum target decreased below the expected hydrodynamic value as the target thickness increased [31]. He attributed this to work hardening plus possible spall. This means that the velocity change in Figure 3g can be used to estimate all the damage done by the shock wave in the copper. We average the late-time trace data to get the final velocity, u_{end}. The energy density difference in the copper, ΔE, is

$$\Delta E(copper) \approx \frac{1}{2}\rho_m\left(u_{start}^2 - u_{end}^2\right), \tag{58}$$

which contains the strain, heat and spall energies.

The scatter between the three types of copper is considerable, and within error, they appear about the same. We next calculate the irreversible heat loss and the Steinberg-Guinan work hardening energy using code-derived strains. We subtract these out to get the spall energy density, which is the largest component in gun-shots. Spall appears to be a function of the impact pressure, P, times the time the pulse is on, τ, i.e. the impulse. Rosenberg, et. al. found no spall in copper at 1.8 GPa and incipient spall at 2.0 GPa, so that a cutoff of P_o = 1.9 GPa seems reasonable [32]. The impulse, J, in the gun shots then is the copper pressure less the cutoff pressure times the pulse length:

$$J = (P_{Cu} - P_o)\tau \,. \tag{59}$$

The pulse length is the time for the shock wave to transverse the flyer twice. It is roughly

$$\tau \approx \frac{3}{3.94 + 1.489 u_{flyer} / 2}. \tag{60}$$

The fit of the spall energy density in kJ cm^{-3} to the impulse is

$$E_{spall} \approx 0.02146J + 0.000463J^2. \tag{61}$$

The impulse data for spall is shown in Figure 3h.

For an explosive, we assume an exponentially-declining pressure wave, which has a time constant υ.

$$J = \int_0^{m\upsilon} \left(P_{Cu} \exp\left(-\frac{t}{\upsilon} \right) - P_o \right) dt = P_{Cu} \upsilon \left[1 - \exp(-m) \right] - P_o \upsilon, \tag{62}$$

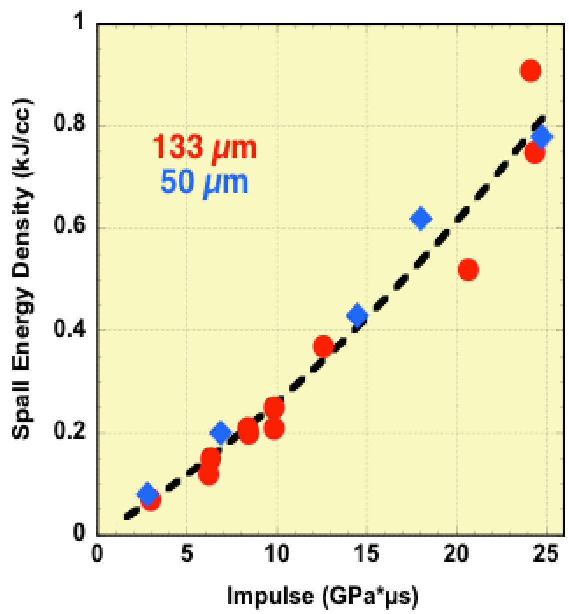

Figure 3h. The spall energy densities for the 50 and 133 μm gun-shot copper samples are a function of the impulse.

where t is time and n is the number of time constants from P to P_o. For LX-17, P is 18 GPa, P_o 1.9 GPa, υ is 0.25 μs so that n is about 2.5 and J equals 3.65 GPa∗μs. From Figure 3h, this puts us at about 0.08 kJ /cc, which is below the 0.1 kJ/cc estimated error of running the code carefully. Because spall turns put to be a small effect, we can ignore the time constant, which we really don't know very well, and create a function that will allow us to correct hundreds of cylinder tests at once on a spreadsheet. We equate the code-calculated maximum copper pressures with the detonation velocities, U_s, used in the problems and we get

$$E_{spall} \approx -0.0973 + 0.0216 U_s. \tag{63}$$

The spall energy density is zero for all detonation velocities below 4.5 mm/μs.

4. Making JWL's

First we need to convert the copper wall velocities to detonation energy densities. For a PDV record, this is done by these steps.

1. Pull up a plot of velocity versus time.
2. Divide the time(X)-axis by the scaling factor. If it is a 2 inch cylinder, divide by 2; a half-inch cylinder, divide by 0.5.
3. Integrate velocity with respect to scaled time to get scaled wall displacement, d.
4. Replot velocity versus scaled displacement.
5. We often cannot take the value at 6 mm (v = 2.4) because of wiggles. To smooth, we set the region 3 to 9 mm and take polynomial fits with a 4 and an 8 power. The resulting combined value at 6 mm is usually good.
6. The 12.5 mm (v = 4.4) and 19 mm (v = 7.0) points usually never have wiggles but sometimes they are noisy. If so, we repeat the same process from 10 < d < 15 and 16 < d < 22 with a fit of 1^{st} or 2^{nd} power.
7. We have been recording a value lately for the 2.5 mm (v = 1.5) point, where wiggles are extreme. So far, we have using 2 < d < 3, 1.5 < d < 3.5 and 1< d < 4 and averaging the results, which are quite scattered. Decades ago, LLNLers fit gigantic polynomials to the entire curve with dubious results, but zone fitting seems safer.
8. We also record the jumpoff velocity, which we can't relate to any relative volume plus the 25.5 mm (v = 10.0) and 32 mm (v = 13.5) points for future reference. At this time, the standard scaled displacement used for making a JWL are 6, 12.5 and 19 mm for v = 2.4, 4.4, and 7.0. Tweaker3 is so constructed that other relative volumes can be used to make JWL's.

The Cylinder test delivers density, detonation velocity and the three adiabat energy densities as input to making a JWL equation-of-state. We next need E_o, the total energy, and It is surprising to learn that it has no true physical meaning. According to the JWL, the detonation energy density will continue toward infinity as the relative volume goes to infinity, so which energy along the way is it? The CHEETAH end-point mechanical energy density can be used, but the truth is that we fiddle with E_o to get the best fit to the measured energy densities. In practice, we start with

$$E_o(kJ/cc) \approx 1.429 + 1.134 * E_d(7.0,\ kJ/cc) \tag{64}$$

$$E_o(Mb) = 0.01429 + 1.134 * E_d(7.0,\ Mb). \tag{65}$$

To make it worse, E_o and ω are intimately connected, and we have to know one to get the other. They are related by the equation

$$\frac{\omega 7^{\omega}}{\omega 10^{\omega}} = \frac{E_o - E_d(10)}{E_o - E_d(7)} \tag{66}$$

which assumes that only the ω-term of the JWL is important from $7 \leq v \leq 10$. We have this equation to get ω, but the ω-E_o approach is still too uncertain.

Everything now goes into Tweaker3. The physical quantities are the initial density ρ_o, the detonation velocity, U_s, and the energy densities $E_d(2.4)$, $E_d(4.4)$, $E_d(7.0)$ and E_o. We put in initial estimates for the non-physical quantities R_1, R_2 and ω, and we shall calculate the non-physical quantities A, B and bhe. The basic equations are as follows.

$$v_{cj} = 1 - \frac{1}{bhe} \tag{67}$$

We next take the "energy form" of the JWL at C-J, which is

$$P_{cj} = A\left(1 - \frac{\omega}{R_1 v_{cj}}\right)\exp\left(-R_1 v_{cj}\right) + B\left(1 - \frac{\omega}{R_2 v_{cj}}\right)\exp\left(-R_2 v_{cj}\right) + \frac{\omega E_s}{v_{cj}} \tag{68}$$

and we combine it with

$$E_s = E_o + \frac{1}{2} P_{cj}(1 - v_{cj}) \tag{69}$$

to get the complicated equation

$$P_{cj} = \frac{A\left(1 - \frac{\omega}{R_1 v_{cj}}\right)\exp\left(-R_1 v_{cj}\right) + B\left(1 - \frac{\omega}{R_2 v_{cj}}\right)\exp\left(-R_2 v_{cj}\right) + \frac{\omega E_o}{v_{cj}}}{1 - \frac{\omega(1 - v_{cj})}{2 v_{cj}}} \quad . \tag{70}$$

The A, B, C-form of the JWL gives

$$C = v_{cj}^{1+\omega}\left[P_{cj} - A\exp\left(-R_1 v_{cj}\right) - B\exp\left(-R_2 v_{cj}\right)\right] \quad . \tag{71}$$

We move away form C-J to the Cylinder test region, where we integrate to energy density

$$E_d = E_o - \left[\frac{A}{R_1}\exp\left(-R_1 v\right) + \frac{B}{R_2}\exp\left(-R_2 v\right) + \frac{C}{\omega v^{\omega}}\right] \ \ at\ \ v = 2.4,\ \ 4.4\ \ and\ \ 7.0 \quad . \tag{72}$$

The derivative of the A, B, C form of the JWL leads to the detonation velocity

$$U_s = \left(\frac{1}{\rho_o}\frac{\partial P}{\partial v}\right)_{cj}^{1/2} = \left\{\frac{1}{\rho_o}\left[AR_1\exp\left(-R_1 v_{cj}\right) + BR_2\exp\left(-R_2 v_{cj}\right) + \frac{(1+\omega)C}{v_{cj}^{2+\omega}}\right]\right\}^{1/2} \tag{73}$$

We end with two C-J pressures

$$P_{cj} = \rho_o U_s^2 (1 - v_{cj}) \tag{74}$$

$$P_{cj} = A\exp\left(-R_1 v_{cj}\right) + B\exp\left(-R_2 v_{cj}\right) + \frac{C}{v_{cj}^{1+\omega}} \quad . \tag{75}$$

We are over-subscribed in equations, so we compare how the detonation velocity has changed and the difference in P_{cj} calculated two different ways. These quality measures should decrease as the calculation proceeds.

$$\alpha code = \frac{100\left[U_s - U_s(initial)\right]}{U_s(initial)} \tag{76}$$

$$\beta code = \frac{100\left[P_{cj}(a) - P_{cj}(b)\right]}{P_{cj}(b)} \tag{77}$$

The "goodness" number tells how good the final fit for energy density is to the original input data

$$\delta = \frac{1}{3}\left\{\frac{E_d(2.4) - E_d(initial2.4)}{E_d(initial2.4)} + \frac{E_d(4.4) - E_d(initial4.4)}{E_d(initial4.4)} + \frac{E_d(7.0) - E_d(initial7.0)}{E_d(initial7.0)}\right\} \tag{78}$$

We now enter a loop of 30 to 50 cycles.

$$bhe(new) = bhe(old) + 0.01\delta \tag{79}$$

$$A(new) = \left(1 - 0.03\alpha code\right)A(old) \tag{80}$$

$$B(new) = \left(1 + 0.05\beta code\right)B(old) \tag{81}$$

The calculation ends when

$$\alpha code,\ \ \beta code \le 0.0002. \tag{82}$$

If we have the three energy densities, how do we use Tweaker3 to make a JWL for something we haven't done before? We enter all the physical quantities, set R_1 = 4.6, R_2 = 1.4 (so that R_1 + R_2 = 6) and ω = 0.28. Use Eq. 64/65 to estimate E_o. We check the goodness of fit, which we want to be 0.3 or better. Suppose it is 0.6 or 1, then

1. change R_1 to (R_1 plus/minus 0.1) and R_2 to (R_2 minus/plus 0.1) in whatever direction works until the goodness minimizes.

2. change E_o up or down by up to 0.05 Mb until the goodness minimizes,

3. change ω by plus/minus 0.01 unti the goodness minimizes.

It is possible that the goodness may never make it 0.3 because the three energy densities didn't have the right proportions. This is as far as you can go unless you suspect one of the energy densities is not correct, and then you can move that in 0.0010 Mb increments.

We can loosely say that R_1 ~ 4.6, R_2 ~ 1.4 for dense explosives and R_1 ~ 5, R_2 ~ 1 for half-dense, but these are just starting points. Now and then you run into someone who likes R_1 ~ 6, R_2 = 2.5 for dense explosives, and there is nothing wrong with that, except the range of adjustable phase space gets smaller as R_1 goes up. From CHEETAH and the DAX test, we can get estimates of the C-J pressure, which are often lower than the ones we get with the JWL. That is because we fit to the three energy densities and let the C-J point fend for itself. There is nothing that can de done about it with the present 3-term equation.

The black Hugoniot represents the overdriven path of the explosive as found in a compressed ball of explosive. The curve is steeper and is fit to overdriven data if it exists. All energy densities are boosted to huge unreal values to try to get the C-J pressure up to the supposed values, but again, 3 terms is not enough and the fit is not always good this way.

5. Hot and Cold Cylinder Shots

Figure 5a shows a two-inch diameter assembly for a 75°C hot shot. The assembly is placed inside the shrapnel catcher with an aluminum foil cover over it. The heaters, seen surrounding the cylinder, are electric coils in ceramic, which are destroyed in every shot. Figure 5b shows the arrangement for a 1-inch diameter cold shot inside a foam plastic box. Cooling is achieved by passing the vapor over liquid nitrogen through the box. In both cases, thermocouples are attached to the top, middle and bottom of the copper cylinder exterior. The final -55° or 75°C is reached in 2-3 hours as determined from the earlier thermal profile test.

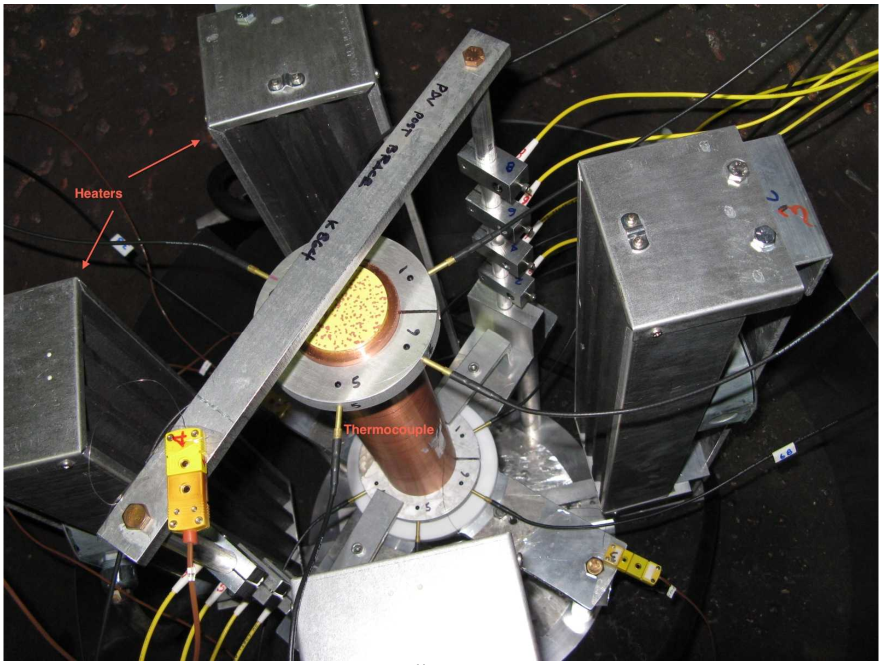

Figure 5a. Hot shot 2-inch diameter LX-17 #864. The PDV probes are shown vertically in the center of the picture.

The thermal profile test is done before the shot to determine how long to wait at temperature until equilibrium is obtained. A Teflon surrogate is placed inside a copper tube as shown in Figure 5c and heated or cooled while measuring multiple thermocouples inside and out. Figure 5d shows the temperature traces, which indicate that a minimum of two hours is needed to equilibrate.

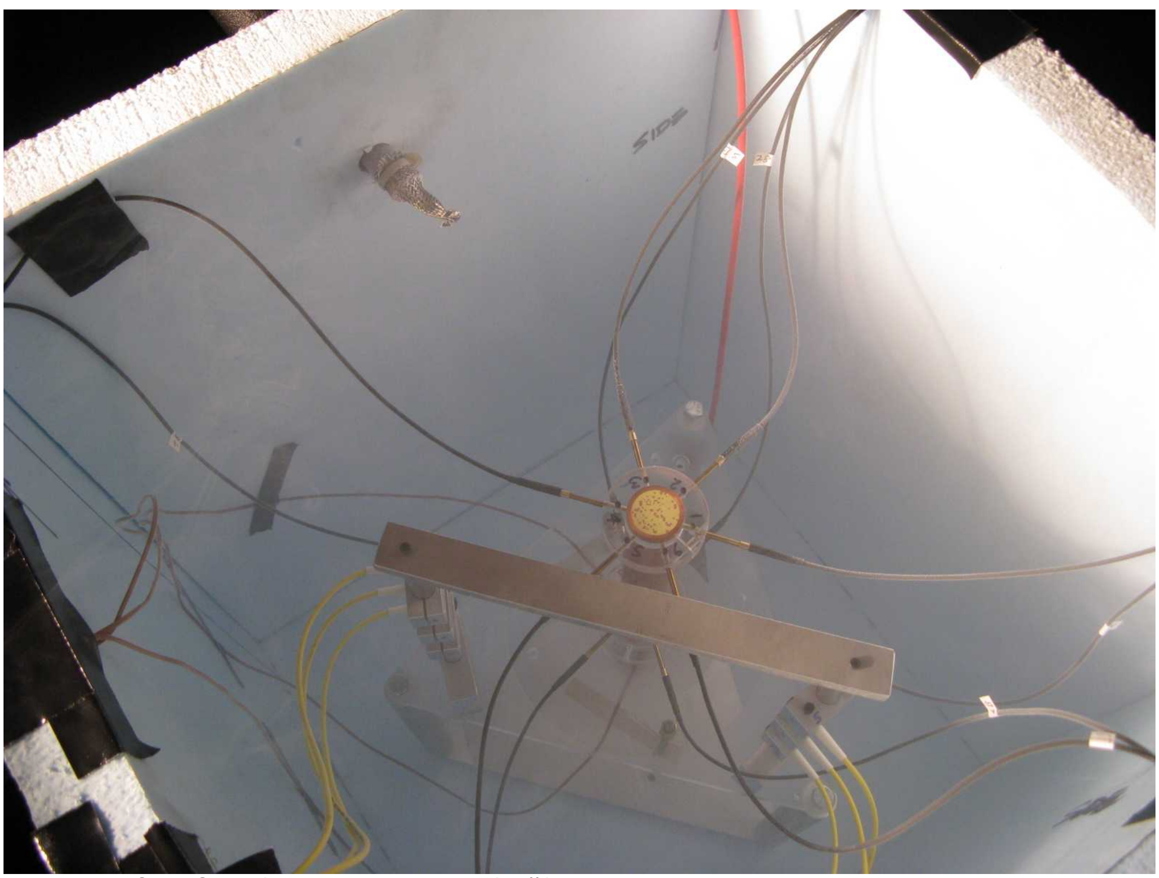
Figure 5b. Cold Shot 1-inch diameter LX-17 #844.

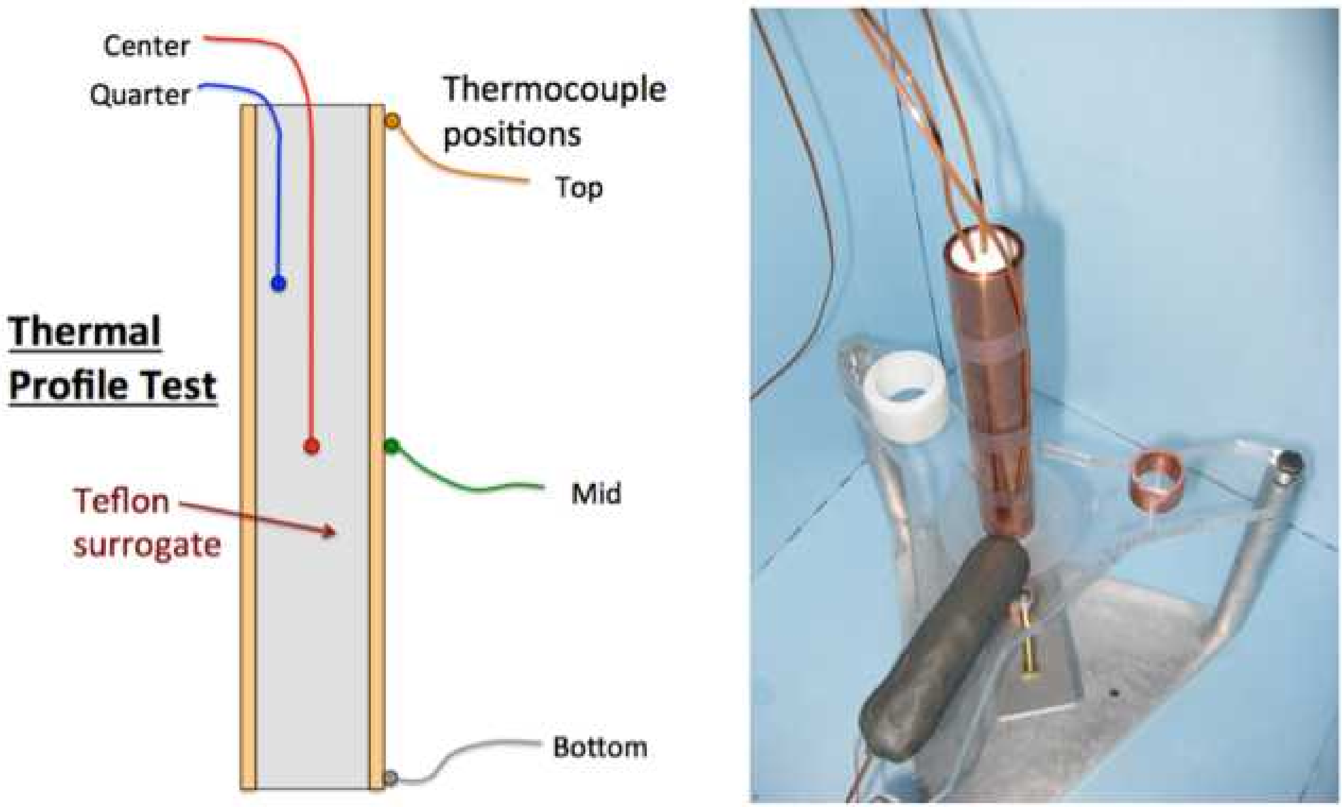

Figure 5c. Thermal profile test for determining how long to wait at temperature before shooting.

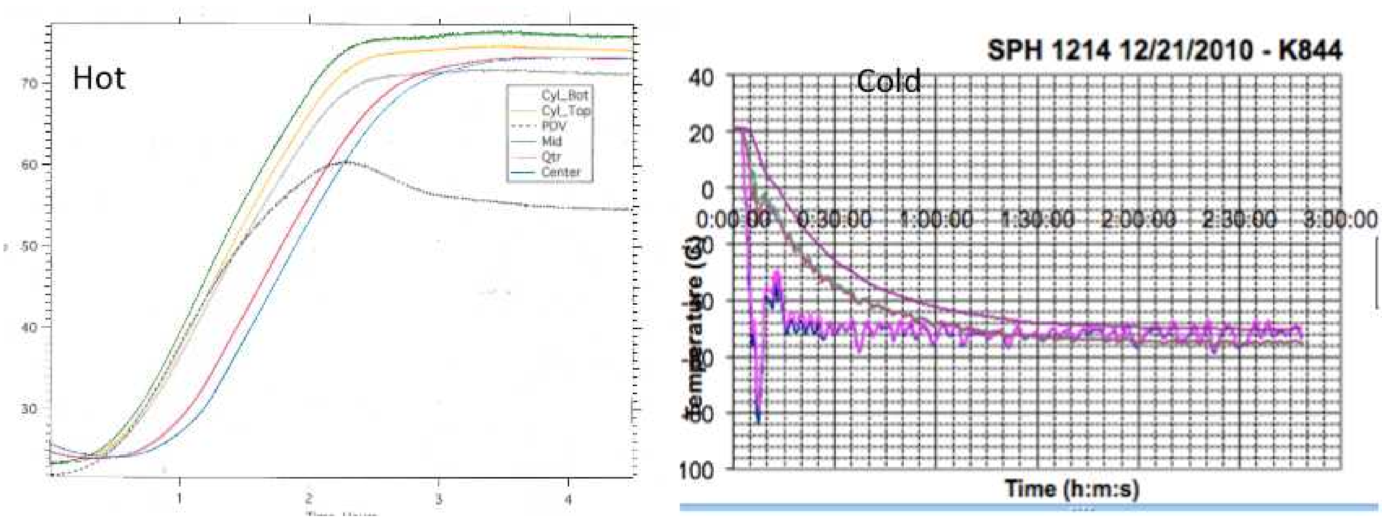

Figure 5d. Thermal profile test results for hot (left) and cold (right) showing that a minimum of two hours is needed for equilibration.

Acknowledgments

This work performed under the auspices of the U. S. Department of Energy by Lawrence Livermore National Laboratory under Contract DE-AC52-07NA27344.

Symbols

A high pressure coefficient in JWL (Mb)
B medium pressure coefficient in JWL (Mb)
bhe variable related to the C-J point (dimensionless)
C low pressure coefficient in JWL (Mb); also mass of explosive per unit length in Gurney equation (g/mm)
C_m coefficient in copper U_s-u_p relation (mm/μs)
d displacement of outer copper edge (mm)
$E_d(v)$ detonation energy density at a relative volume (kJ/cc)
E_g energy density of gas (kJ/cc)
E_{heat} irreversible heat loss density (kJ/cc)
E_{spall} spall energy density (kJ/cc)
E_{strain} work hardening energy density (kJ/cc)
E_w energy density of wall (kJ/cc)
E_o total energy in JWL (Mb)
ΔE total energy density lost in copper (kJ/cc)
g air gap energy multiplier (dimensionless)
G/G_o shear modulus ratio (dimensionless)
J impulse (GPa*μs)
K coefficient for instantaneous strain (dimensionless)
k power for instantaneous strain (dimensionless)
m number of time constants passed in explosive (dimensionless)
M mass of metal per unit length in Gurney equation (g/mm)
n power in the S-G model (dimensionless)
P_{cj} pressure at C-J point (GPa or Mb)
P_{Cu} maximum shock pressure in the copper (GPa)
P_o cut-off pressure for spall (GPa)
r radius (mm)
R_1 high pressure coefficient in JWL (dimensionless)
R_2 medium pressure coefficient in JWL (dimensionless)
S later scaled explosive radius (mm)
S_o initial scaled explosive radius (mm)
S_{1m} coefficient in metal U_s-u_p relation (dimensionless)
S-G Steinberg-Guinan model
t time (μs)
U_s detonation velocity (mm/μs)
u velocity (mm/μs)
u_α Doppler velocity of copper wall seen by laser probe (mm/μs)
u_β wall velocity along copper particle velocity vector (mm/μs)
u_{end} final velocity of copper target (mm/μs)
u_{flyer} velocity of copper flyer (mm/μs)
$u(gap)$ copper wall velocity with air gap effects (mm/μs)
u_m copper wall velocity perpendicular to tilted wall (mm/μs)
u_{start} initial velocity of copper target (mm/μs)
u_o phase velocity of copper wall (mm/μs)
v relative volume in explosive (dimensionless)
v_{cj} relative volume at C-J point (dimensionless)
v_{Cu} relative volume in copper (dimensionless)
X_o initial scaled copper wall thickness (mm)
X later scaled copper wall thickness (mm)

xdot copper wall velocity in the code (mm/µs)

X_{gap} initial scaled air gap width (mm)

Y_o initial yield strength of copper in S-G (GPa)

Y later yield strength of copper in S-G model (GPa)

ydot copper wall velocity in the code (mm/µs)

Y_{max} ultimate yield strength of copper in S-G (GPa)

α angle of wall velocity seen by laser probe (degrees)

αcode calculation limit in Tweaker (dimensionless)

βcode calculation limit in Tweaker (dimensionless)

β strain coefficient in the S-G model (dimensionless) ; also angle defining copper wall particle velocity (degrees)

δ goodness of fit to measured energy data in Tweaker (dimensionless)

ε plastic strain caused by a shock (dimensionless)

ρ explosive density at later time (g/cc)

ρ_o initial explosive density (g/cc)

ρ_m initial metal density (g/cc)

Θ tilt angle of the cylinder wall (degrees)

τ pulse time in the gun shot (µs)

υ time constant In explosive Taylor wave (µs)

ω low pressure coefficient in JWL (dimensionless)

References

[1] J. W. Kury, H. C. Hornig, E. L. Lee, L. McDonnel, D. L. Ornellas, M. Finger, F. M. Strange and M. L. Wilkens, "Metal Acceleration by Chemical Explosives," *Proceedings of the Fourth Symposium (International) on Detonation*, White Oak, MD, October 12-15, 1965, pp. 3-12.

[2] P. C. Souers and J. W. Kury, "Comparison of Cylinder Data and Code Calculations for Homogeneous Explosives," *Propellants, Explosives, Pyrotechnics, 18*, 175-183 (1993).

[3] C. R. Barrett, J. L. Lytton and O. D. Sherby, "Effect of Grain Size and Annealing Treatment on Steady-State Creep of Copper," *Transactions Metallurgical Society AIME 239*, 170-180 (1967).

[4] Bruce Cunningham and Lisa Lauderbach, LLNL, private communication, 2011.

[5] F. C. Nix and D. MacNair, "The Thermal Expansion of Pure Metals: Copper, Gold, Aluminum, Nickel and Iron," *Physical Review 60*, 597-605 (1941)

[6] P. Clark Souers and Roger Minich, "Cylinder Test Correction for Copper Work Hardening and Spall," *Propellants, Explosives, Pyrotechnics,* accepted, 2014.

[7] O. T. Strand, D. R. Goosman, C. Martinez, T. L. Whitworth and W. W. Kuhlow, A Novel System for High-Speed Velocimetry using Heterodyne Techniques, *Revs. Sci. Intrs. 77*, 083108 (2006).

[8] [McMillan] C. F. McMillan, et al., "Velocimetry of Fast Surfaces Using Fabry-Perot Interferometry," *Rev. Sci. Instrum. 59*, 1 (1988).

[9] R. W. Gurney, *The Initial Velocities of Fragments from Bombs, Shells and Grenades*, Army Ballistic Research Laboratory, report BRL 405 (1943).

[10] John E. Reaugh and P. Clark Souers, "A Constant-Density Gurney Approach to the Cylinder Test," *Propellants, Explosives, Pyrotechnics, 29*, 124-128 (2004).

[11] P. C. Souers, Raul Garza, Howard Hornig, Lisa Lauderbach, Cinda Owens and Peter Vitello, "Metal Angle Correction in the Cylinder Test," *Propellants, Explosives, Pyrotechnics, 36* [1], 9-15 (2011).

[12] P. C. Souers, L. Lauderbach, R. Garza, L. Ferranti, Jr. and P. Vitello, "Upgraded Analytical Model of the Cylinder test," *Propellants, Explosives, Pyrotechnics 38* [3], 419-424 (2013).

[13] P. C. Souers and L. C. Haselman, Jr., *Detonation Equation of State at LLNL,1993*, Lawrence Livermore National Laboratory, report UCRL-ID0116113 (1994), pp. 4-2 to 4-4, 4-8.

[14] D. J. Steinberg, S. G. Cochran and M. W. Guinan, "A Constitutive Model for Metals applicable at High-Strain Rate, *J. Appl. Phys. 51* [3], 1498-1504 (1980).

[15] D. J. Steinberg, *Equation of State and Strength Properties of Selected Materials*, Lawrence Livermore National Laboratory, Livermore, CA, report UCRL-MA-106439, (1991).

[16] R. G. McQueen and S. P. Marsh, Ultimate Yield Strength of Copper, *J. Applied Physics 33* [2], 654-665 (1962).

[17] D. Hayes, R. S. Hixson and R. G. McQueen, "High Pressure Elastic Properties, Solid-Liquid Phase Boundary and Liquid Equation of State from Release Wave Measurements in Shock-Loaded Copper," *Shock Compression of Condensed Matter-1999*, M. D. Furnish, ed., American Institute of Physics, Melville, NY, Conference Proceedings 505, pp. 483- 488 (2000).

[18] W. Tong and R. J. Clifton, "Pressure-Shear Impact Investigation of Strain-Rate History Effects in Oxygen-Free High-Conductivity Copper," *J. Mech. Phys. Solids 40* [6], 1251-1294 (1992).

[19] L. C. Chhabildas and J. R. Asay, "Time-Resolved Wave Profile Measurements in Copper to Megabar Pressures," *Proceedings of Eighth AIRAPT and 19th EHPRG*, Uppsala, Sweden, T. Johanisson, et. al., pp. 183-188 (1981).

[20] H. Huang and J. R. Asay, "Reshock Response of shock deformed Aluminum," *J. Applied Physics 100*, 043514 (2006).

[21] H. Huang and J. R. Asay, "Reshock and Release Response of Aluminum Single Crystal," *J. Applied Physics 101*, 063550 (2007).

[22] H. Huang and J. R. Asay, "Compressive Strength of Shocked Aluminum at Stresses of 4-22 GPa," *Shock Compression of Condensed Matter-2005*, M. D. Furnish, T. P. Russell and C. T. White, eds., American Institute of Physics (2005); *J. Applied Physics 98*, 033524 (2005).

[23] W. H. Gourdin, "Analysis and Assessment of Electromagnetic Ring Expansion as a High-Strain-Rate test," *J. Applied Physics 65*, 411-422 (1989).

[24] W. H. Gourdin, *Constitutive Properties of Copper and Tantalum at High Rates of Tensile Strain: Expanding Ring Results*, Lawrence Livermore National Laboratory, report UCRL-98812 (1988).

[25] W. J. Murphy, A. Higginbotham, G. Kimminau, B. Barbrel, E. M. Bringa, J. Hawreliak, R. Kodama, M. Koenig, W. McBarron, M. A. Meyers, B. Nagler, N. Ozaki, N. Park, B. Remington, S. Rothman, S. M. Vinko, T. Whitcher and J. S. Wark, "The Strength of Single Crystal Copper under uniaxial Shock Compression at 100 GPa," *J. Phys: Condensed Matter 22*, 065404, Figure 1 (2010).

[26] R. W. Armstrong and F. J. Zerilli, High Rate Straining of Tantalum and Copper," *J. Phys. D Applied Physics 43*, 492002 (5 pages, 2010).

[27] *Mie-Gruneison Equation of State*, Wikipedia, March, 2013.

[28] B. Banerjee, *An Evaluation of Plastic Flow Stress Models for the Simulation of High-Temperature and High Strain-Rate Deformation of Metals,* University of Utah, posted on the net, http://www.eng.utah.edu, 2013.

[29] Ya. A. Zeldovich and Yu. P. Raizer, *Physics of Shock Waves and High-Temperature Hydrodynamic Phenomena*, W. D. Hayes and R. F. Probstein, eds. Academic Press, New York, volume II, pp. 710-711 (1967).

[30] R. W. Minich, J. C. Cazamias, M. Kumar and A. J. Schwartz, "Effect of Microstructural Length Scales on Spall Behavior of Copper," *Metallurgical and Materials Transactions A 35A*, 2663-2673 (2004).

[31] D. R. Curran, “Nonhydrodynamic Attenuation of Shock Waves in Aluminum,” *J. Applied Physics 34* [9], 2677-2685 (1963).

[32] Z. Rosenberg, M. Mayseless, Y. Partom and A. A. Betser, “Spall Studies in Copper,” *J. Applied Physics 58* [2], 1083-1086 (1985).